Weld metal microstructure prediction from fundamentals of transport phenomena and phase transformation theory

Z. Yang and T. DebRoy

Modelling the evolution of weld metal microstructure requires knowledge of cooling rates at various locations in the fusion zone. In the recent past, significant advances have been made in the calculation of transient three-dimensional temperature fields, considering convective heat transfer and fluid flow in the weld pool. However, very little effort has been made to use these accurate cooling rates to understand fusion zone microstructures. The present paper demonstrates the advantages of microstructure calculations using fundamentals of transport phenomena and phase transformation theory. The velocity and temperature fields, the shape and size of the fusion zone, and the cooling rates at different locations were calculated by solution of the equations for conservation of mass, momentum, and energy in three dimensions. The time–temperature transformation (TTT) diagrams were calculated for a series of steels with varying carbon and manganese contents using a phase transformation model. The TTT diagrams and the computed cooling rates were then used to obtain the continuous cooling transformation (CCT) diagrams and the microstructures. The computed volume fractions of the various microstructural constituents were then compared with the experimental results. Good agreement between the computed and the experimental results indicates significant promise for predicting weld microstructure from the fundamental principles of transport phenomena and phase transformation theory.

The authors are in the Department of Materials Science and Engineering, the Pennsylvania State University, PA, USA. *Manuscript received 26 November 1996.*

INTRODUCTION

Weldment properties are influenced by its macro- and microstructures. During the fusion welding process, the interaction of the material and the heat source leads to rapid heating, melting, and vigorous circulation of the molten metal in the weld pool. The circulation is primarily driven by buoyancy, surface tension, and, when electric current is used, electromagnetic forces. The resulting mass and heat transfer and fluid flow affect the size and shape of the weld pool, the cooling rates, and the kinetics and extent of various solid state transformation reactions in the fusion and heat affected zones. The process variables affect the weldment composition and cooling rates that, in turn, affect the weldment microstructure. Since there are a large number of welding variables, it is usually a painstaking endeavour to establish a satisfactory welding procedure capable of producing a desired weldment structure. The target structure and properties are commonly obtained by adjusting variables such as the heat input, preheat temperature, and other welding variables by trial and error. Because of the complexities of the fusion welding process, understanding the composition and microstructure of the weldment remains a major objective in producing defect free, structurally sound, and reliable welds.

An accurate prediction of the thermal cycle in the weld metal is a prerequisite for reliable prediction of the weld metal microstructure. The direct measurement of temperature profiles in the weld pool is difficult and non-contact techniques for the measurement of weld pool surface temperatures are still evolving. Previous models for the calculation of time–temperature history involved solution of the equation for conservation of energy[1,2] without consideration of the convection in the weld pool. Fluid flow in the weld pool can significantly affect the cooling rates. In recent years, significant progress has been made in the understanding of heat transfer and fluid flow in the weld pool.[3–8] For example, weld pool shape and size of over 200 conduction mode laser spot welds fabricated under various conditions were in good agreement with the corresponding values obtained from a heat transfer and fluid flow model.[9,10] Evolution of the weld pool geometry during subkilowatt and multikilowatt conduction mode laser welding could be predicted for various concentrations of sulphur in steel, laser power values, power densities, and welding conditions.[10] The peak temperatures in the weld pool[11] obtained from the measurement of relative evaporation rates, the measured vaporisation rates of the alloying elements, and the cross-sectional areas of the weld pools[12] were in good agreement with the theoretical results.[13] Furthermore, simple features of the solidification structure, such as the secondary dendrite arm spacings, have been satisfactorily predicted from the cooling rates obtained using a heat transfer and fluid flow model.[5] However, the cooling rates at various weldment monitoring locations obtained from such comprehensive models have not been extensively used to calculate weldment microstructures. Initial efforts toward this end are presented in Refs. 14 and 15.

The aim of the present work was to predict microstructures of steel weldments from fundamentals of transport phenomena and phase transformation theory. The heat transfer and fluid flow in the last pass of a multipass weld fabricated by the manual metal arc welding process were investigated by numerically solving the equations for conservation of mass, momentum, and energy in the weld pool in transient three-dimensional form. Fluid flow arising from surface tension and electromagnetic and buoyancy forces was considered. The cooling rates at various locations were computed as a function of time. The time–temperature transformation (TTT) diagram was calculated using an available phase transformation model.[16,17] The cooling rates calculated from the comprehensive fluid flow and heat transfer model and the TTT diagram calculated by the

phase transformation model were combined to obtain the continuous cooling transformation (CCT) diagram. The volume fractions of the various constituents in the microstructure were then calculated and compared with the experimental results.

TRANSIENT TEMPERATURE FIELD CALCULATIONS

The temperature fields were determined by numerical solution of the equations for conservation of mass, momentum, and energy in three-dimensional form. The details of the solution procedure are available elsewhere.[8] Only the important assumptions and the salient features of the calculations are presented here. The effects of Marangoni, electromagnetic, and buoyancy forces were considered in the solution procedure and the weld pool surface was assumed to be flat for simplicity. Fluctuations of the mass of the weld pool owing to droplet impingement were approximated by a constant time averaged mass of the liquid metal in the weld pool. Energy transfer both from the arc and from the droplets was considered. The transient nature of the energy transfer by the droplets was approximated by a time averaged value of energy transport rate and the arc was assumed to have a Gaussian energy density distribution. The absorption coefficient was determined from the results of an independent investigation.

The numerical solution of transient three-dimensional equations for conservation of mass, momentum, and energy is time consuming and expensive. In the present work, the transient problem was transformed into a steady state problem by solving in a coordinate system which moves with the heat source. In the moving coordinate system, the velocity and enthalpy fields are independent of time. As a consequence, the time required for computation is reduced significantly. The velocity transformation used and the transformed continuity, momentum, and energy equations can be expressed by[8]

$$V = \bar{V} + V_s \quad \ldots \quad (1)$$

$$\nabla \cdot V = 0 \quad \ldots \quad (2)$$

$$\rho \nabla \cdot (\overline{VV}) = -\nabla P + \mu \nabla \cdot (\nabla \bar{V}) + S_V - \rho \nabla \cdot (V_s \bar{V}) \quad \ldots \quad (3)$$

$$\rho \nabla \cdot (\bar{V} h) = \nabla \cdot (\nabla hk/C_P) + S_l + S_h - \rho \nabla \cdot (V_s h) \quad \ldots \quad (4)$$

where V, $\bar{V}$, and V_s are the velocity at any point, convective component of the velocity, and the welding velocity respectively, ρ is the density, μ is the viscosity, P is the effective pressure, C_P is specific heat, h is the sensible heat, k is thermal conductivity, S_V is the source term that takes into account the combined effect of buoyancy force, Marangoni stress, and electromagnetic force, S_h is the source term that takes into account the heat input from the welding source and the convective and radiative heat loss, and S_l is the source term that accounts for latent heat of melting and convective transport of latent heat.

The governing equations were represented by finite difference equations and solved iteratively on a line by line basis using a tridiagonal matrix algorithm. The details of the procedure are described elsewhere.[18] A $55 \times 30 \times 25$ grid system was used in the calculations and spatially non-uniform grids were used for maximum resolution of variables.

After the solution of the transformed momentum and energy equations, temperature as a function of time at different locations (x, y, z) within the weldment can be calculated from the relation

$$T(x, y, z, t_2) = \frac{T(\xi_2, y, z) - T(\xi_1, y, z)}{\xi_2 - \xi_1} U_s(t_2 - t_1) + T(x, y, z, t_1) \quad \ldots \quad (5)$$

where $T(\xi_2, y, z)$ and $T(\xi_1, y, z)$ are the steady state temperatures at coordinates (ξ_2, y, z) and (ξ_1, y, z) respectively, $\xi_2 - \xi_1$ is the distance travelled by the arc in time $t_2 - t_1$, U_s is the welding speed, and $T(x, y, z, t_2)$ and $T(x, y, z, t_1)$ are the temperatures at times t_1 and t_2 respectively.

Since many complex physical processes take place during welding, to keep the computational processes tractable, only the essential physical processes have been modelled. As some observable effects like the deformation of the free surface have not been considered, these assumptions may appear to be somewhat restrictive. However, the appropriateness of an assumption depends on the information desired from modelling. Comparison of the predicted results with the experimental data provides a test of the assumptions. The cooling rate data obtained from the model were found to be in good agreement with the corresponding measured values for different welding conditions.[19] Thus, the cooling rates used are believed to be trustworthy.

In another set of calculations, the cooling rates between 1073 and 773 K were obtained by a semiempirical formula, established by regression of experimental results[20]

$$dT/dt = c_1(T - T_i)^{c_2}/q\eta \quad \ldots \quad (6)$$

where T is temperature, t is time, q is the energy input per unit length, η is the energy transfer efficiency, T_i is interpass temperature, and c_1 and c_2 are adjustable constants according to different welding processes. This formula has been used to predict the cooling rates in the temperature range 1073–773 K. For best results, c_1 and c_2 have to be determined for each set of experimental conditions. When some conditions change, e.g. the welding process, geometry, and the shape and size of the specimen, new values of c_1 and c_2 have to be determined from experimental data. Furthermore, this formula assumes that c_1 and c_2 are independent of locations in the fusion zone. Therefore, the cooling rates obtained from this formula can not be used to predict either the spatial variation of microstructure within the fusion zone or the changes in microstructure resulting from the variation of welding variables.

Table 1 Composition and austenite grain size parameter L for selected Fe–C–Mn low alloy steels[24]

	Content, wt-%									
Alloy	C	Si	Mn	P	S	Al	N	Ti	O	L^*, μm
1	0·030	0·45	0·78	0·010	0·013	0·009	95	0·014	336	65
2	0·059	0·34	0·77	0·010	0·010	0·007	66	0·011	306	71
3	0·059	0·33	1·09	0·010	0·008	0·007	64	0·010	310	65
4	0·059	0·30	1·44	0·010	0·006	0·007	65	0·009	305	60
5	0·065	0·33	1·83	0·010	0·003	0·007	76	0·009	291	48
6	0·090	0·41	0·78	0·010	0·013	0·003	36	0·014	421	45
7	0·089	0·35	1·18	0·010	0·011	0·008	73	0·012	404	45
8	0·088	0·37	1·59	0·010	0·011	0·003	77	0·012	491	45
9	0·12	0·43	0·86	0·014	0·011	0·005	54	0·015	329	36

* Mean lineal intercept measured normal to length axis of grains.

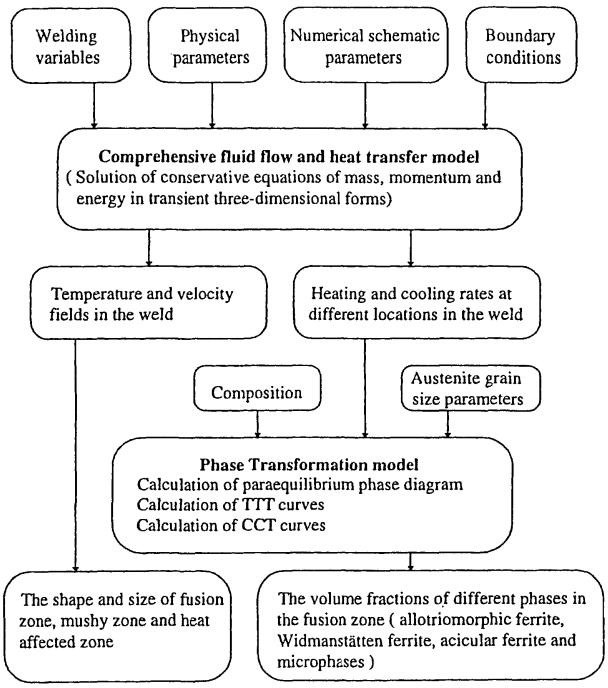

1 Flow chart of model

PHASE TRANSFORMATION MODEL

The high temperature gradients at the fusion boundary cause the δ ferrite grains to grow epitaxially from the base metal into the weld zone during solidification of low alloy steels.[21] The resulting grains have a columnar morphology, with their major axis following the direction of maximum heat flow. On further cooling, δ ferrite transforms to austenite and then, as the temperature decreases further, austenite decomposes to a series of ferrites (allotriomorphic, Widmanstätten, and acicular ferrites), bainite, or martensite. For low alloy steels, the final microstructure is determined by the austenite decomposition process in the temperature range 1073–773 K. The allotriomorphic ferrite is the first phase transformed from austenite. It nucleates at the austenite grain boundary and grows by a diffusional mechanism. On further cooling, the Widmanstätten ferrite nucleates at the allotriomorphic ferrite/austenite boundary and grows by a displacive mechanism.[16] Acicular ferrite forms after Widmanstätten ferrite as the temperature decreases further.

The phase transformation model used in the present work is described in detail by Bhadeshia *et al.*[16] The calculations were performed as described in Ref. 22. Scheil's 'additive rule' was used to construct a CCT diagram from the TTT diagram and the cooling rate.[23] The comprehensive fluid flow and heat transfer model[8] and the phase transformation model[16] were used to predict the weld microstructure. The flow chart of the model is shown in Fig. 1.

Table 2 Parameters used for calculation of velocity and temperature fields

Liquid temperature, K	1780·0
Solid temperature, K	1742·0
Density of liquid metal, kg m^{-3}	7200·0
Viscosity of liquid, kg m^{-1} s^{-1}	$6{\cdot}0 \times 10^{-3}$
Thermal conductivity of solid, J m^{-1} s^{-1} K^{-1}	27·1
Thermal conductivity of liquid, J m^{-1} s^{-1} K^{-1}	83·6
Specific heat of solid, J kg^{-1} K^{-1}	702·0
Specific heat of liquid, J kg^{-1} K^{-1}	806·7
Latent heat of melting, J kg^{-1}	$267{\cdot}6 \times 10^{3}$
Temperature coefficient of surface tension, N m^{-1} K^{-1}	$-0{\cdot}43 \times 10^{-3}$

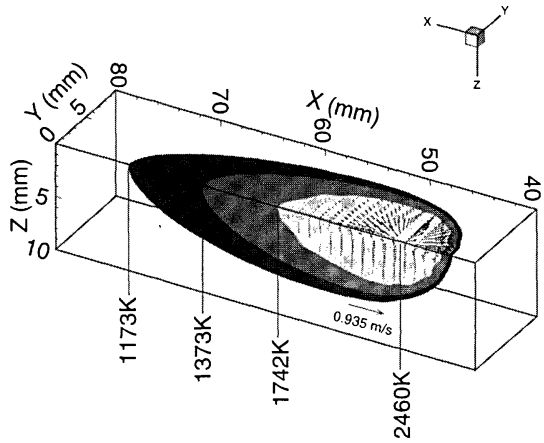

2 Calculated temperature and velocity fields in weld specimen

PREDICTION OF C–Mn WELD METAL MICROSTRUCTURE

The model was used to predict the effects of carbon and manganese on the weld microstructure. The calculated results were then compared with independent experimental results[24] available in the literature, which used a current of 180 A, voltage of 23 V, welding speed of 0·004 m s^{-1}, and a T_i value of 250°C. The alloy compositions and the experimentally determined austenite grain size parameters are given in Table 1, while the physical property values used for the calculations of velocity and temperature fields are given in Table 2.

RESULTS AND DISCUSSION

The calculated temperature and velocity fields in the weld specimen are shown in Fig. 2. The general features of the calculated temperature field are consistent with the results reported in the literature.[4] In front of the heat source, the temperature gradient is larger than behind the heat source. The high temperature gradient results in slightly higher liquid metal velocities in front of the heat source than behind the heat source. At the surface of the weld pool, the liquid metal moves from the centre to the periphery. This is expected for alloys with a very low concentration of surface active elements and consequently a negative temperature coefficient of surface tension.

The calculated temperature profiles and thermal cycles at different locations in the weld are shown in Figs. 3 and 4 respectively. From Fig. 3 the shape and size of the fusion zone, the mushy zone (two phase, solid/liquid zone), and the heat affected zone can be determined. The temperature contour corresponding to a solidus temperature of 1742 K

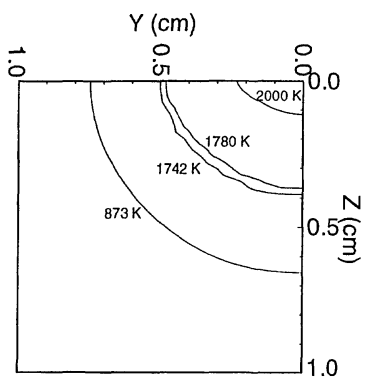

3 Calculated temperature profiles at different locations in weld

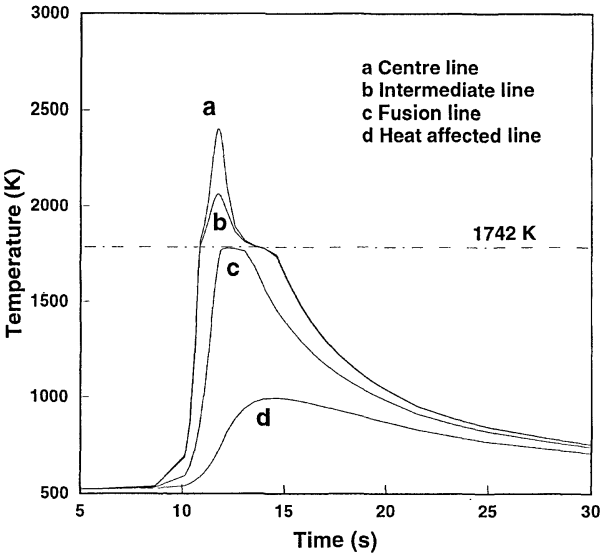

4 Calculated thermal cycles at different locations in weld

represents the fusion line of the weld. The mushy zone, which is located between the solidus temperature line and liquidus temperature line (1780 K), is identified. It can be seen from Fig. 4 that the peak temperatures at different locations are not attained at the same time. The time to reach the peak temperature at a specified location depends on its distance from the axis of the heat source.

Cooling rates between 1073 and 773 K at different locations calculated by the comprehensive fluid flow and heat transfer model are compared with that calculated by a widely used semiempirical formula[20] in Fig. 5. It can be seen that the cooling rates in the fusion zone calculated by the model are faster than that obtained from the empirical formula. Furthermore, in the temperature range 1073–773 K, the difference in the cooling rates at different locations in the fusion zone is small for the conditions of welding.

The calculated TTT diagrams for different carbon and manganese contents are shown in Fig. 6. The upper and lower 'C' curves in the diagram represent the initial time for diffusional transformation, e.g. the formation of allotriomorphic ferrite, and displacive transformation, e.g. the

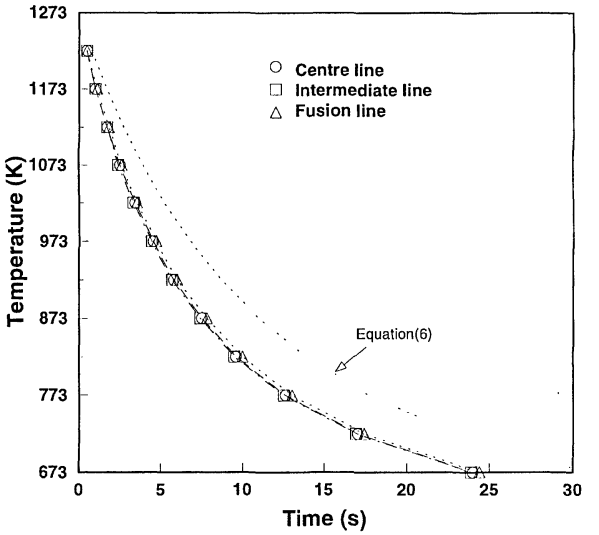

5 Comparison of calculated cooling rates from comprehensive model and cooling rates from semiempirical formula

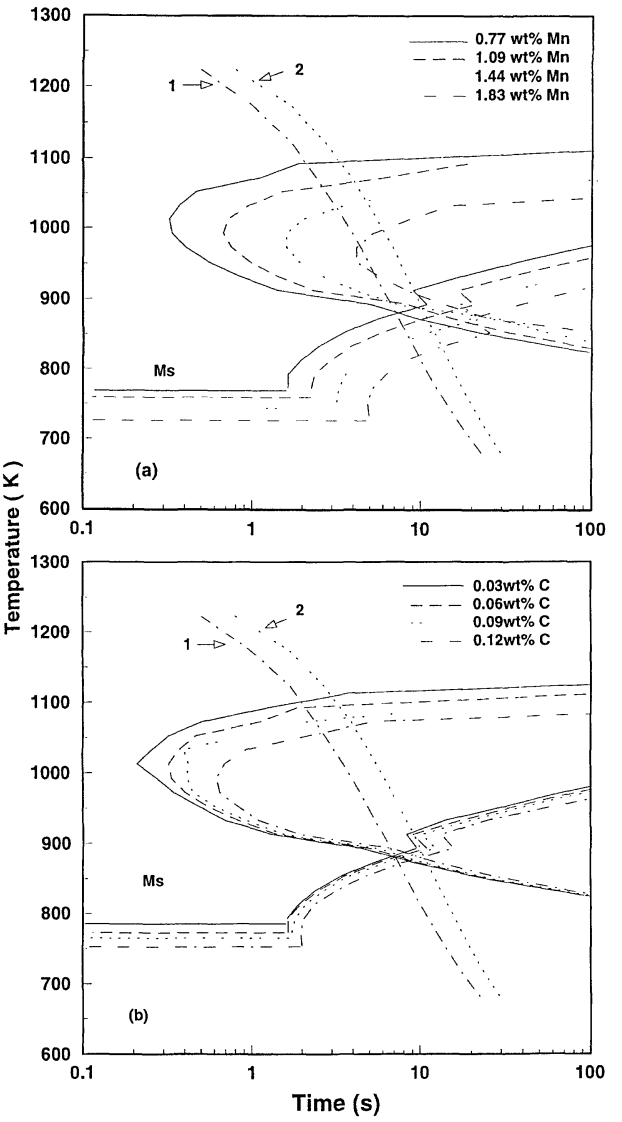

a with 0·06 wt-%C; *b* with 0·8 wt-%Mn

6 Calculated TTT diagrams for selected C–Mn low alloy steels: cooling curves 1 and 2 obtained from model and semiempirical formula respectively

formation of Widmanstätten, acicular ferrite, or bainite, respectively. The horizontal lines represent the martensite start temperatures M_s. From Fig. 6, it is clear that both the upper and lower 'C' curves shift to the right and the M_s temperature decreases as the carbon or the manganese content increases. This is expected, because both carbon and manganese significantly promote hardenability of steels. Furthermore, at a constant temperature, as the carbon or manganese content increases, the time necessary for the initiation of allotriomorphic ferrite and Widmanstätten ferrite formation is delayed. The 'additive rule' is used to construct a CCT diagram from the TTT diagram and the computed cooling rate. The details are provided in Ref. 23.

The calculated and experimental volume fractions of the various phases in the weld microstructure are given in Table 3. Two sets of calculated results obtained by using two computed cooling rates are shown. Cooling rates were obtained from the model and the semiempirical equation. Comparisons of the two sets of calculated and the experimental results are shown in Fig. 7. In general, the calculated results are in good agreement with the experimental results. The agreement between the experimental data and the model prediction was significantly better than that between

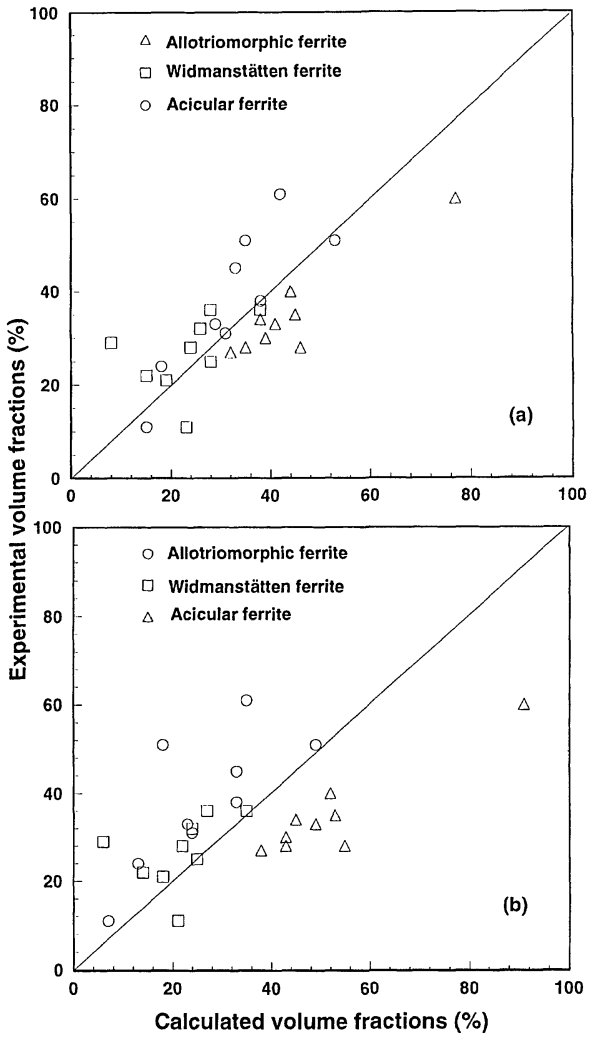

a for cooling rate from model; *b* for cooling rate from semiempirical formula

7 Comparison of calculated phase volume fractions with experimental results

the data and the calculated results based on the cooling rates obtained from the empirical equation.[20]

In general, the calculated volume fractions of allotriomorphic ferrite are slightly higher than the experimental values. In the calculations, the retardation in growth kinetics as a result of the overlap of carbon concentration fields near several particles[22] was ignored. This effect, known as the soft impingement effect, becomes more pronounced as the volume fraction of ferrite increases. Since the soft impingement effect was not considered, the phase transformation model overpredicted the growth rate of allotriomorphic ferrite. As a result, the calculated volume fractions of Widmanstätten and acicular ferrites are lower than the experimental values. Other uncertainties include empirical kinetic parameters and inaccuracies in the calculated cooling rates. On the whole, the good agreement achieved between the experimental and the predicted volume fractions indicates promise for predicting microstructural variations resulting from systematic variations in welding parameters.

EPILOGUE

Methodologies for the calculation of convective heat flow and weld metal cooling rates are now well accepted. Reliable commercial computer programs for solution of the equations for conservation of mass, heat, and momentum have been adapted to achieve high efficiency and accuracy of the numerical solution. Two main factors affect the accuracy of the calculated cooling rates. First, because the welding processes are complex, certain simplifications are necessary to make the computational task tractable. Second, appropriate thermophysical data are not always readily available. In view of these difficulties, large comprehensive models to calculate cooling rates must be verified by comparing model predictions with experimental data. The model used in the present work has been tested extensively against experimental data of over 200 weld pool geometries[9,10] and many other parameters such as the cooling rates,[19] secondary dendrite area spacings,[5] and vaporisation rates of various alloying elements.[13]

The main lesson to be learnt from the results presented here is not merely that the calculated cooling rates are more accurate than the corresponding values obtained from an empirical equation. In many instances, when an engineer is in search of a theory, simple models can be attractive. However, the approach adopted here is just the opposite: higher accuracy is achieved by including a more realistic and detailed description of the physical processes in welding. The most important feature of this approach is its usefulness in understanding trends in microstructure resulting from variations in both welding variables and weld metal composition based on the fundamentals of transport phenomena and phase transformation theory. The work described represents an initial step towards this end.

Table 3 Comparison of calculated volume fractions using model (A) and semiempirical formula (B) with experimental volume fractions[24] (C)

	V_α*			V_w†			V_a‡ + V_m§		
Alloy	A	B	C	A	B	C	A	B	C
1	77	91	60	8	2	29	15	7	11
2	44	52	40	38	35	36	18	13	24
3	41	49	33	28	27	36	31	24	31
4	39	43	30	28	25	25	33	33	45
5	35	43	28	23	21	11	42	35	61
6	45	53	35	26	24	32	29	23	33
7	38	45	34	24	22	28	38	33	38
8	32	38	27	15	14	22	53	49	51
9	46	55	28	19	18	21	35	28	51

* Allotriomorphic ferrite.
† Widmanstätten ferrite.
‡ Acicular ferrite.
§ Microphases.

CONCLUSIONS

A comprehensive fluid flow and heat transfer model, based on the fundamentals of transport phenomena, has been used to determine the velocity and temperature fields, the shape and size of the fusion zone, and the cooling rates at different locations in the weldment. An available phase transformation model has been used to calculate the TTT diagram for each alloy composition. The calculated cooling rate and the TTT diagram were then combined to predict the development of the weld microstructure during continuous cooling. The calculated volume fractions of the phases in the weld microstructures of the selected Fe–C–Mn weld metals agreed well with the experimental results. Furthermore, the experimentally determined volume fractions of the different phases were in relatively better agreement with the model predictions than with those obtained using a more common semiempirical cooling rate formula. This agreement indicates significant promise for predicting weld microstructure from the fundamental principles of transport phenomena and phase transformation theory.

ACKNOWLEDGEMENTS

This work was supported by the US Department of Energy, Office of Basic Energy Sciences, Division of Materials Science under grant number DE–FG02–84ER45158. The authors would like to thank Dr K. Mundra and Dr S. S. Babu for their comments on the manuscript. The authors are grateful to Dr H. K. D. H. Bhadeshia for help with the microstructure calculations.

REFERENCES

1. D. ROSENTHAL: *Weld. J.*, 1941, **20**, 2208.
2. C. M. ADAMS, Jr: *Weld. J.*, 1958, **37**, 211.
3. C. CHAN, J. MAZUMDER, and M. M. CHEN: *Metall. Trans. A*, 1984, **15A**, 2175.
4. S. KOU and Y. H. WANG; *Metall. Trans. A*, 1986, **17A**, 2265.
5. A. PAUL and T. DEBROY: *Metall. Trans. B*, 1988, **19B**, 851.
6. K. MUNDRA, T. DEBROY, T. ZACHARIA, and S. A. DAVID: *Weld. J. Res. Suppl.*, 1992, **71**, (9), 313s.
7. T. DEBROY and S. A. DAVID: *Rev. Mod. Phys.*, 1995, **67**, (1), 85.
8. K. MUNDRA, T. DEBROY, and K. KELKAR: *Numer. Heat Transfer A*, 1996, **29**, 115.
9. W. PITSCHENEDER, T. DEBROY, K. MUNDRA, and R. EBNER: Proc. 4th Int. Conf. on Trends in Welding Research, (ed. H. B. Smartt *et al.*), 627; 1996, Materials Park, OH, ASM International.
10. W. PITSCHENEDER, T. DEBROY, K. MUNDRA, and R. EBNER: *Weld. J. Res. Suppl.*, 1996, **75**, (3), 71s.
11. P. A. A. KHAN and T. DEBROY: *Metall. Trans. B*, 1985, **16B**, 853.
12. P. A. A. KHAN, T. DEBROY, and S. A. DAVID; *Weld. J. Res. Suppl.*, 1988, **67**, (1), 1s.
13. K. MUNDRA and T. DEBROY: *Metall. Trans. B*, 1993, **24B**, 145.
14. K. MUNDRA, T. DEBROY, S. S. BABU, and S. A. DAVID: Proc. 4th Int. Conf. on Trends in Welding Research, (ed. H. B. Smartt *et al.*), 259–264; 1996, Materials Park, OH, ASM International.
15. K. MUNDRA, T. DEBROY, S. S. BABU, and S. A. DAVID: *Weld. J. Res. Suppl.*, to be published.
16. H. K. D. H. BHADESHIA, L.-E. SVENSSON, and B. GRETOFT: *Acta Metall.*, 1985, **33**, 1271.
17. H. K. D. H. BHADESHIA: in 'International trends in welding science and technology', (ed. S. A. David and J. M. Vitek), 213; 1993, Materials Park, OH, ASM International.
18. S. V. PATANKAR: 'Numerical heat transfer and fluid flow'; 1980, New York, Hemisphere Publishing.
19. K. MUNDRA, J. M. BLACKBURN, and T. DEBROY: *Sci. Technol. Weld. Joining*, to be published.
20. L.-E. SVENSSON, B. GRETOFT, and H. K. D. H. BHADESHIA: *Scand. J. Metall.*, 1986, **15**, 97.
21. G. J. DAVIES and J. G. GARLAND: *Int. Met. Rev.*, 1975, **20**, 83.
22. H. K. D. H. BHADESHIA and L.-E. SVENSSON: in 'Mathematical modelling of weld phenomena', (ed. H. Cerjak and K. E. Easterling), 109; 1993, London, The Institute of Materials.
23. M. TAKAHASHI and H. K. D. H. BHADESHIA: *Mater. Trans., JIM*, 1991, **32**, (8), 689.
24. L.-E. SVENSSON and B. GRETOFT: *Weld. J. Res. Suppl.*, 1990, **12**, 454.